Since January 2020 Elsevier has created a COVID-19 resource centre with free information in English and Mandarin on the novel coronavirus COVID-19. The COVID-19 resource centre is hosted on Elsevier Connect, the company's public news and information website.

Journal of the Indian Chemical Society 99 (2022) 100416

Contents lists available at ScienceDirect

Journal of the Indian Chemical Society

journal homepage: www.journals.elsevier.com/journal-of-the-indian-chemical-society

Antioxidant properties, anti- SARS-CoV-2 study, collagenase and elastase inhibition effects, anti-human lung cancer potential of some phenolic compounds

Liang Wei [a], Zhenhui Liao [a], Haili Ma [a], Jingjing Wei [b,*], Chenyuan Peng [a,**]

[a] Department of Pulmonary and Critical Care Medicine, Liyuan Hospital of Tongji Medical College of Huazhong University of Science & Technology, Wuhan, 430077, China

[b] Dapartment of Intensive Care Unit, Liyuan Hospital of Tongji Medical College of Huazhong University of Science & Technology, Wuhan, 430077, China

ARTICLE INFO

Keywords:
Molecular docking
ADME/T
Anti-oxidant
Anti-Lung cancer
Enzyme inhibition

ABSTRACT

Lung cancer is one of the main reasons for death worldwide. The natural compounds with anti-lung cancer potential are of main interest and are considered a very promising alternative to replace or raise the efficiency of conventional drugs. Diethylstilbestrol, Enterodiol, Enterolactone, Flavokawain A, Flavokawain B, and Flavokawain C compounds showed excellent to good inhibitory activities against studied these enzymes with IC_{50} values in ranging between 9.66 ± 1.52 to 121.20 ± 15.87 μM for collagenase and 11.06 ± 1.87 to 27.31 ± 4.673 μM for elastase. Also, these compounds had In vitro anti-lung cancer activities. Comparison of the chemical and biological activities of the studied molecules was made by theoretical calculations. Gaussian sofware program was used for chemical activity. The Maestro molecular docking calculations were made to compare their biochemical activities. Afterwards, ADME/T calculations of the molecules were made.

1. Introduction

Lung cancer is the cancer type with the highest mortality rate in the world and is responsible for approximately 1.2 million deaths per year. It is the second most common after prostate cancer in men and breast cancer in women. Etiological cause and epidemiological data show that lung cancer is a preventable disease [1,2]. Because smoking, occupation, air pollution, and radiation are the most important causes of lung cancer development. In addition, it is stated that previous lung disease sequelae, diet, viral infections, gender, genetic and immunological factors may also play a role in the etiology. According to the 2004 classification of the World Health Organization (WHO), the histological subgroups of lung cancer are majorly squamous cell cancer, small cell cancer, adenocarcinoma, large cell cancer, mixed adenosquamous cell cancer and cancer of mucous gland cells (mucoepidermoid cancer, adenoid cystic carcinoma, carcinoid tumor) [3,4]. The rate of squamous cell cancer and adenocarcinoma varies depending on the type of cigarette used in cigarette consumption in the community. In developed countries where light smoking is widely used and its use is increasing proportionally, the most common lung cancer cell type is adenocarcinoma due to the causative effect of nitrosamines. Lung cancer can cause many symptoms, clinical and laboratory findings in patients due to the systemic nature of the disease [5]. These are related to tumor localization, growth and extension characteristics, and metabolic activity. Patients may present with symptoms such as cough, weight loss, shortness of breath, hemoptysis, bone pain, fever, chest pain, clubbing, weakness, superior vena cava syndrome, dysphagia, and wheezing. Imaging methods are widely used for staging determination, which is very necessary in for determining the prognosis and diagnosis and treatment of patients with lung cancer [6,7].

Elastases are a class of serine proteases that have the ability to can cleave elastin, an important protein of connective tissue. elastases; It is a group of serine proteases that are abundant in vertebrate tissues, especially in the lungs, arteries, skin, and ligaments, and have the ability to can degrade elastin, an important connective tissue protein. These proteases include pancreatic elastase, neutrophil elastase (leukocyte elastase), macrophage elastase, and fibroblast elastase [8,9]. The dermis, which is responsible for the flexibility and strength of the skin, is located in the middle layer of the skin and consists of connective tissue elements. As a result of the breakdown of elastin and collagen, which are

* Corresponding author.
** Corresponding author.
E-mail addresses: Wjjlyyy0803@163.com (J. Wei), p373048507@163.com (C. Peng).

https://doi.org/10.1016/j.jics.2022.100416
Received 8 December 2021; Received in revised form 1 February 2022; Accepted 5 March 2022
Available online 6 March 2022

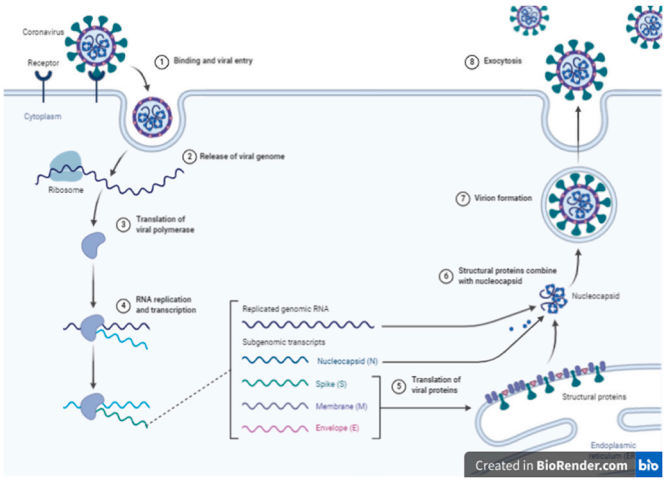

Fig. 1. Life cycle of coronavirus.

Table 1
IC_{50} values of some phenolic compounds on collagenase and elastase enzymes.

NO	Compounds	Collagenase	Elastase
		IC50 (μM)	IC50 (μM)
1	Diethylstilbestrol	121.20 ± 15.87	13.28 ± 2.78
2	Enterodiol	104.41 ± 11.30	11.06 ± 1.87
3	Enterolactone	9.66 ± 1.52	22.46 ± 4.08
4	Flavokawain A	66.31 ± 7.95	27.31 ± 4.67
5	Flavokawain B	71.07 ± 15.98	20.13 ± 2.36
6	Flavokawain C	62.05 ± 9.43	17.60 ± 1.68
	Phosphoramidon[a]	101.37 ± 14.76	–
	N-(Methoxysuccinyl)-Ala-Ala-Pro-Val-chloromethyl ketone[a]	–	30.55 ± 3.25

[a] These compounds are controls.

Table 2
Anti-oxidant properties of studies molecules.

Molecule	Atom	BDE	IP	PDE	PA	ETE
Enterodiol	H44	45.80	154.22	206.09	357.83	2.48
	H37	60.64	154.22	220.93	377.69	−2.54
	H48	60.64	154.22	220.93	377.69	−2.54
	H43	45.80	154.22	206.09	357.83	2.48
Enterolactone	H39	42.79	174.86	182.44	351.80	5.49
	H40	43.46	174.86	183.10	353.59	4.37
Flavokawain C	H31	53.37	145.14	222.74	346.53	21.34
	H38	52.74	145.14	222.11	350.52	16.72

the main elements of connective tissue, with elastase and collagenase enzymes, wrinkles accompanying skin aging occur. Elastase activity increases with increasing age, and this causes a decrease in the elastic properties of the skin and sagging skin with aging. Inhibition of this enzyme has attracted attention in recent years due to its positive effects on both the prevention of skin aging and connective tissue diseases [10, 11].

Studying the chemical properties of molecules by theoretical calculations has become very popular today. It is possible to obtain important information before many experimental procedures are made with the calculations made. In the theoretical calculations, firstly, the anti-oxidant properties of the molecules were examined with the Gaussian

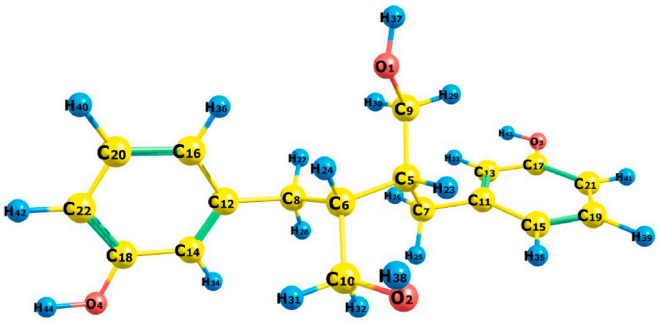

Fig. 2. Atomic labeling of enterodiol molecule.

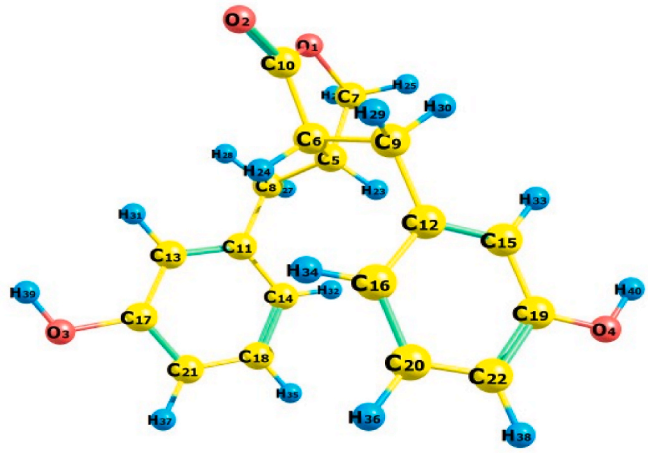

Fig. 3. Atomic labeling of enterolactone molecule.

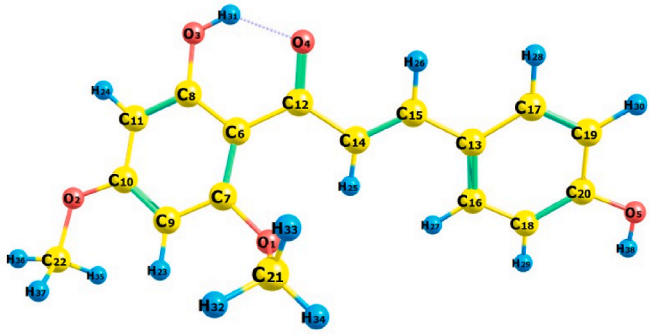

Fig. 4. Atomic labeling of flavokawain C molecule.

software program. The Clostridium histolyticum colH collagenase enzyme (pdb: 4U6T) [12]. The chemical structures of three polycystic kidney-disease like domains from *Clostridium histolyticum* collagenase enzymes such as ColH and ColG and elastase enzyme from porcine pancreatic (pdb: 9EST) [13] has have been used. Apart from its enzyme proteins, the inhibitory activities of SARS-CoV-2 virus, which is the major infectious disease of today, against the main protease protein (pdb: 7BUY) [14] were compared. It is very important to obtain a good inhibitor against this most contagious disease today. Finally, their activities against the anti-oxidant protein Human peroxiredoxin 5 protein (pdb: 1HD2) [15] were compared. Finally, for the anti-oxidant calculations made by DFT calculations of the molecules, it was confirmed by molecular docking calculations.

The entry of the SARS-CoV-2 virus into human metabolism, how it moves inside the cell, and finally its exit by reproducing inside the cell

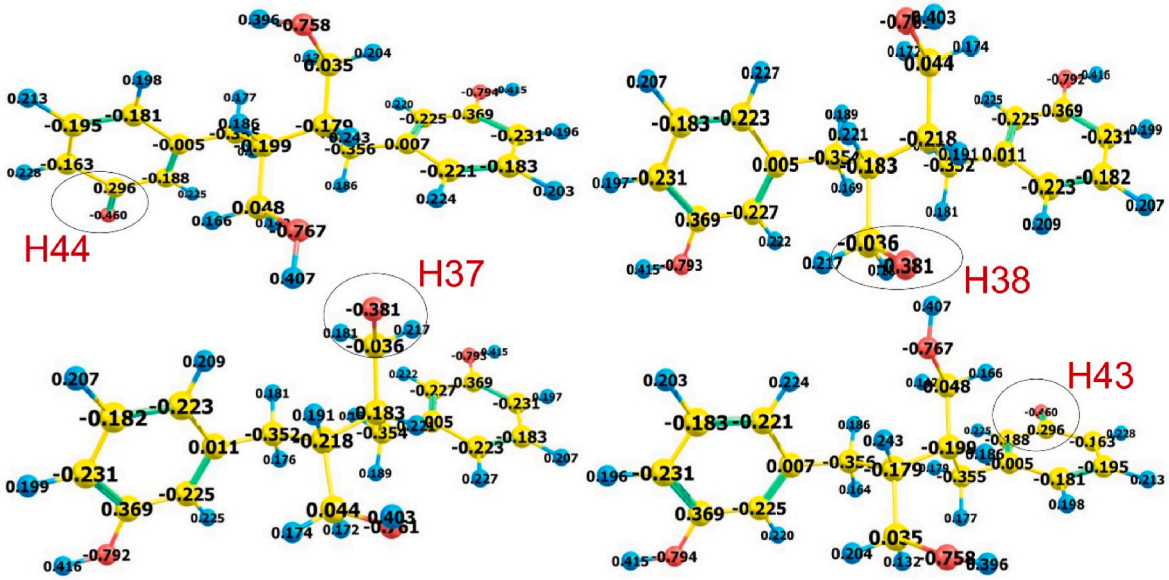

Fig. 5. Spin density distributions of enterodiol molecule.

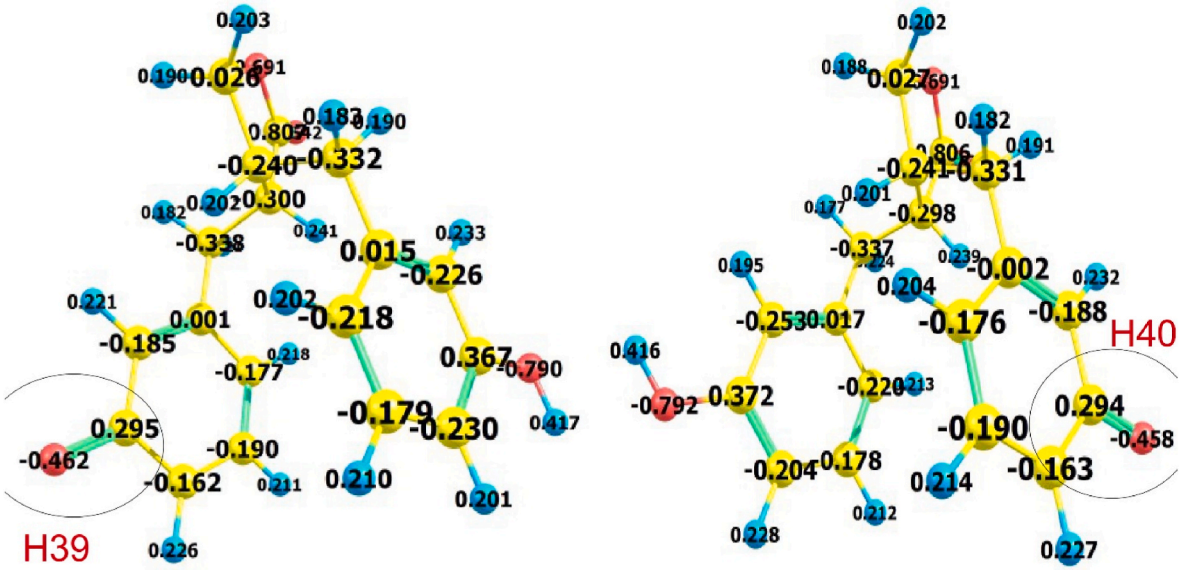

Fig. 6. Spin density distributions of Enterolactone molecule.

[16] are shown in detail in Fig. 1, created with Biorender.

2. Experimental

2.1. Materials

We used Collagenase, elastase, N-succinyl-ala-ala-ala-*p*-nitroanilide (STANA), Tris-HCl, DMSO, MTT in this study.

2.2. Enzymes

Modified inhibitory effect on collagenase enzyme Thring et al. (2009) [17] was investigated spectrophotometrically using the assay. The 50 μL of the solution containing 0.8 U/mL collagenases was taken, 50 μL of plant extracts and chemical substance solutions at different concentrations prepared on it were added. This method was performed according to previous studies. The absorbance values of the sample solutions and control solution were read at 340 nm in the UV spectrophotometer against the blank [18]. Experiments were repeated 2 times. The amount of IC_{50} value substance required for the collagenase enzyme to have a 50% inhibition effect, and also calculated with the regression equation obtained from the linear section of the curve drawn by applying the concentration to the abscess in the graph and the % enzyme inhibition data to the ordinate [19].

Elastase inhibitory activity was determined spectrophotometrically confirming to the method of Moon et al. (2010) [20]. In our study, 50 μL of each plant extract prepared with DMSO at different concentrations (0.00001–0.01 μg/mL) was taken. 0.9 mL of Tris-HCl buffer solution with 0.2 M pH of 7.8 was added to it. 50 μL of enzyme was added to the control solution. The same amount of distilled water was used instead of the enzyme for the blank. Blank, control and sample solutions were incubated for 15 min at 37 °C. After the first incubation, 50 μL of 5 mM N-succinyl-ala-ala-ala-*p*-nitroanilide (STANA) was added to all tubes and incubated again at 37 °C for 30 min [21]. The absorbance values of

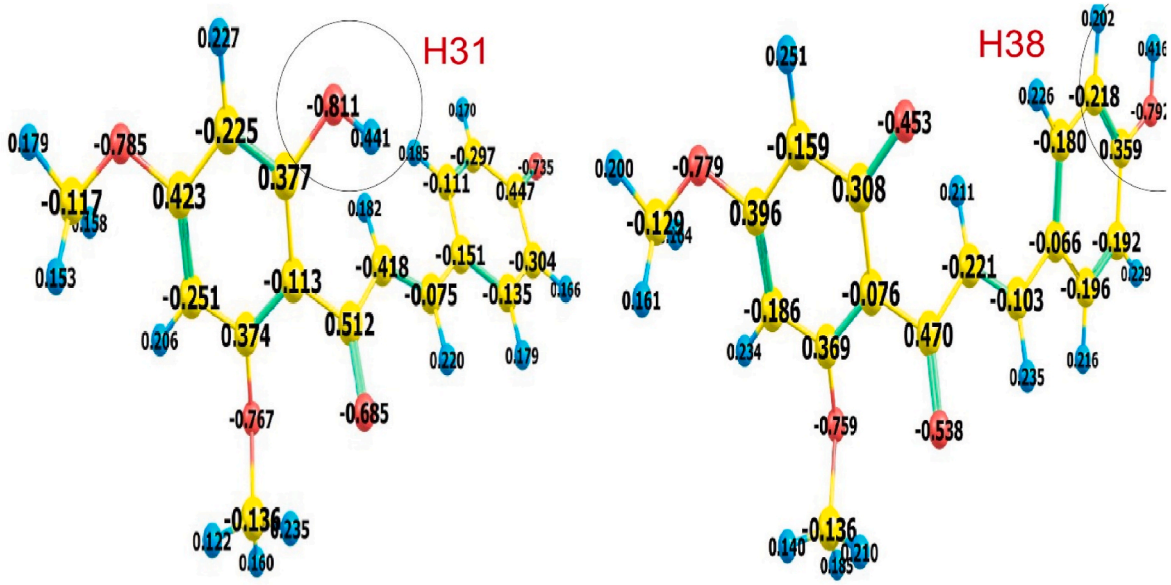

Fig. 7. Spin density distributions of Flavokawain C molecule.

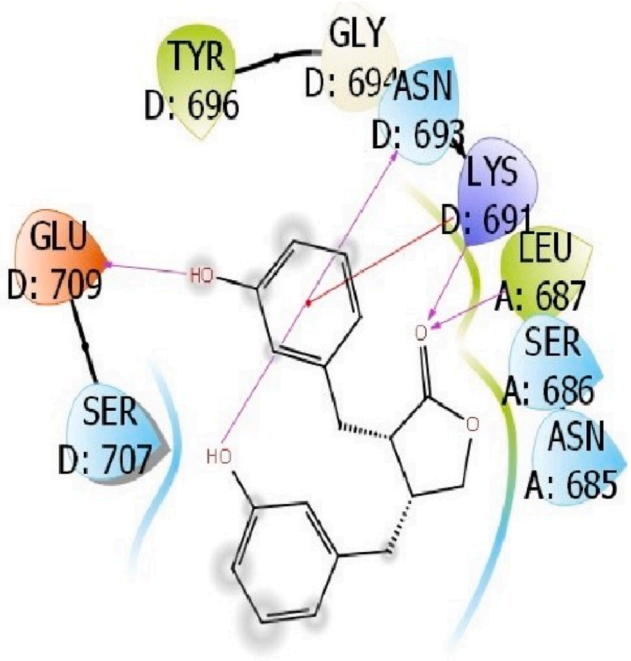

Fig. 8. Presentation interactions of Enterolactone Diglicoside with collagenases protein.

the sample and control solutions were read at 410 nm against the blank in the spectrophotometer [22]. In the study, anti-elastase inhibition activity experiments of compounds prepared at different concentrations were repeated 3 times. The IC_{50} value of the elastase enzyme was calculated from the regression equation obtained from the linear

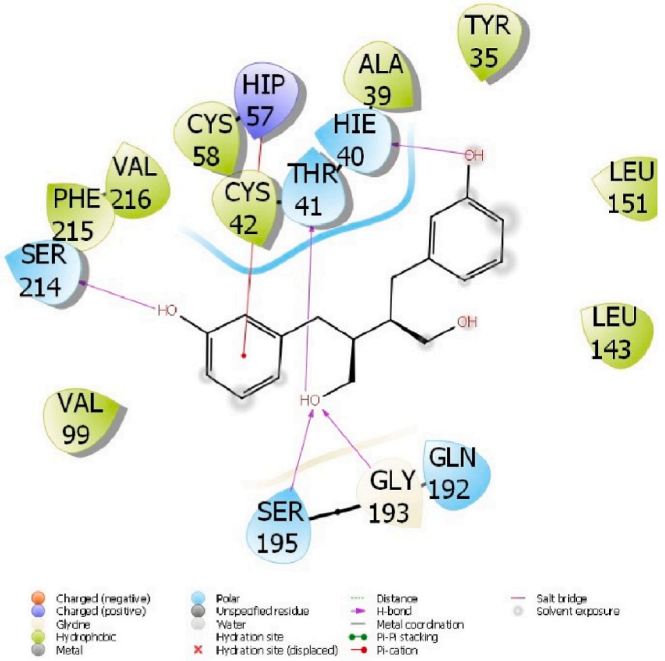

Fig. 9. Presentation interactions of Enterodiol with elastase enzym

segment of the curve drawn by applying the concentration to abscess and % elastase inhibition data to the ordinate [23].

2.3. Theoretical calculations

With theoretical calculations, anti-oxidant calculations of molecules are made in more than one step. In these multiple steps: ionization potential (IP), bond dissociation enthalpy (BDE), proton affinity (PA), proton dissociation enthalpy (PDE), and electron transfer enthalpy (ETE) parameters are calculated [24–28]. In this study, the anti-oxidant calculations of the three molecules with the highest experimental activity were made. The anti-oxidant calculations made consist of 3 stages. In the first stage, the hydrogen atom transfer mechanism (HAT) numerical value is calculated.

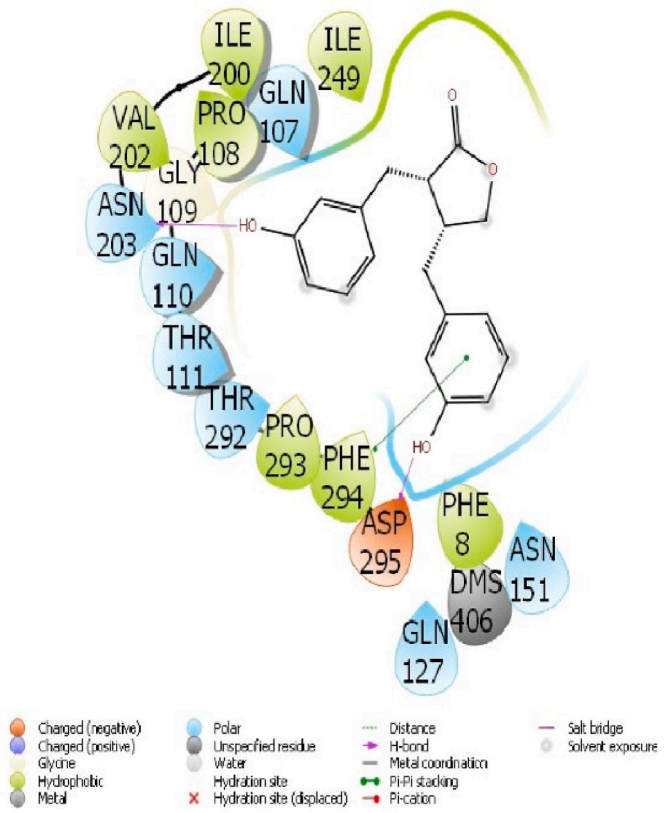

Fig. 10. Presentation interactions of Enterolactone with SARS-CoV-2 virus.

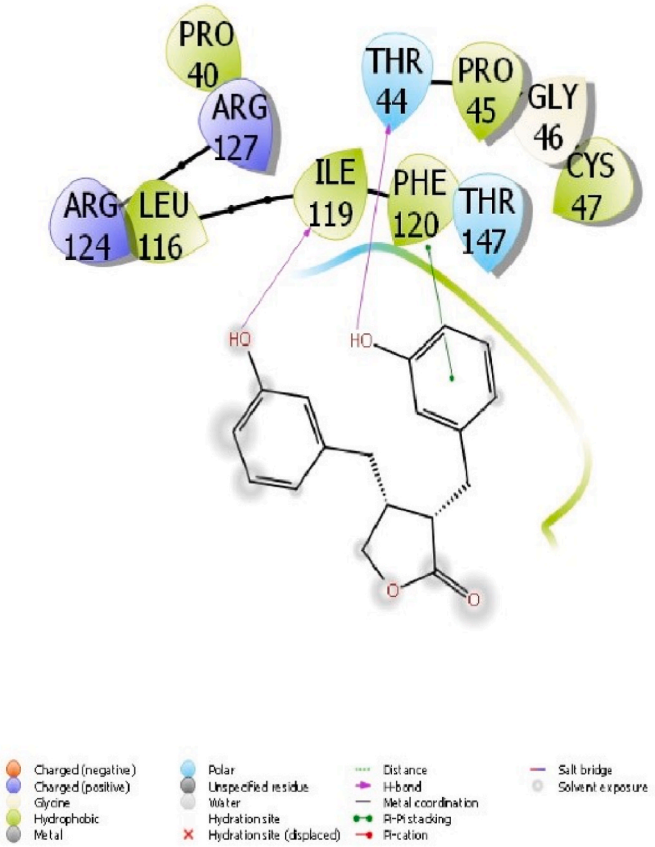

Fig. 11. Presentation interactions of Enterolactone with SARS-CoV-2 virus.

In the first reaction, a hydrogen is cleaved from the antioxidant molecule (AH) as a result of the interaction of the free radical molecule ($R^{\cdot}$) with the antioxidant molecule. The anti-oxidant molecule turns the antioxidant into a free radical ($A^{\cdot}$) form by removing a hydrogen. To compare the activities of the antioxidant molecule, it is necessary to calculate the bond dissociation enthalpy (BDE) of the A-H bond.

$$R^{\cdot} + AH \rightarrow RH + A^{\cdot} \quad (1)$$

Single electron transfer-proton transfer (SET-PT) value is calculated for the above mechanisms. In this mechanism, it consists of two stages. In the first mechanism, the proton transfer occurs, and then the electron moves away from AH.

$$R^{\cdot} + AH \rightarrow R^{-} + AH^{+\cdot} \quad (2)$$

$$AH^{+\cdot} \rightarrow H^{+} + A^{+} \quad (3)$$

In the third stage, firstly the ionization potential (IP) from the $AH^{+\cdot}$ cation radical and secondly the proton dissociation enthalpy (PDE) mechanisms. These two mechanisms occurring are called SPLET (Sequential proton loss electron transfer) mechanism.

$$AH \rightarrow A^{-} + H^{+} \quad (4)$$

$$A^{-} + H^{+} + R^{\cdot} \rightarrow A^{\cdot} + RH \quad (5)$$

Gaussian software program was used to calculate the enthalpy energy values in these mechanisms. In the calculations, DFT calculations were used on the Hartree-Fock (HF) level 6–31++G(d,p) basis set [29, 30].

In addition, molecular modeling calculations were made to compare the biochemical activities of the studied compounds and their activities were compared. As a result of these calculations, many parameters were found from the calculations. The numerical value of these parameters gives a lot of significant information about the activities of compounds. Molecular modeling calculations to compare the biochemical activities of compounds were made using the Maestro Molecular docking platform (version 12.2) by Schrödinger [31]. Calculations are made as a result of combining many modules. The first module used includes the preparation of the studied molecules for calculations. At first, optimized structures of the molecules were obtained from the Gaussian software program [32]. It was then prepared for calculations using the LigPrep module [33] using optimized structures of the molecules. In another module, studied four proteins with the protein preparation module [34] were prepared for calculations. The Glide ligand docking module was used to interact with the molecules and protein prepared later. Finally, the Qik-prop module [35] of the Schrödinger software was used to predict the effects and responses on human metabolism as working molecules as drugs. With this calculation, the absorption of the molecules into the human body, their distribution in the body, their effects and reactions in the metabolism, their excretion from the metabolism and their toxic effects are examined by ADME/T analysis (distribution, excretion, absorption, metabolism, and toxicity).

2.4. Cytotoxicity assay

The MTT method was performed as explained previously. Cells were seeded onto a 96-well plate at a concentration of 104 cells/well and allowed to adhere overnight. Five replicates were prepared for each therapy and cultured for 48 or 72 h. After 20 mL of MTT (5 mg/mL) was added to each well, the cells were cultured for another 4 h. The supernatant was discarded. After 150 mL of DMSO was added to each well, the samples were incubated at 37 °C for 30 min and then swirled for 10 min. The absorbance at 570 nm was measured using a microplate reader. Experiments were repeated three times [36].

Table 3
Numerical values of the docking parameters of molecule against enzymes.

Collagenase	Diethylstilbestrol	Enterodiol	Enterolactone	Flavokawain A	Flavokawain B	Flavokawain C
Docking Score	–	−5.13	−5.78	−4.44	−3.64	−5.06
Glide ligand efficiency	–	−0.23	−0.26	−0.19	−0.17	−0.23
Glide hbond	–	−0.58	−0.74	−0.11	−0.19	−0.38
Glide evdw	–	−16.08	−14.36	−24.05	−19.97	−22.41
Glide ecoul	–	−22.03	−22.20	−9.61	−8.10	−12.07
Glide emodel	–	−47.92	−47.38	−40.36	−32.05	−43.00
Glide energy	–	−38.10	−36.56	−33.66	−28.08	−34.48
Glide einternal	–	8.68	8.87	6.62	6.57	5.13
Glide posenum	–	43	311	392	10	316
Elastase	**Diethylstilbestrol**	**Enterodiol**	**Enterolactone**	**Flavokawain A**	**Flavokawain B**	**Flavokawain C**
Docking Score	−3.49	−6.68	−5.64	−4.47	−4.35	−4.95
Glide ligand efficiency	−0.17	−0.30	−0.26	−0.19	−0.21	−0.23
Glide hbond	0.00	−1.39	−0.82	−0.32	0.00	−0.32
Glide evdw	−19.51	−23.22	−26.15	−22.60	−24.52	−20.30
Glide ecoul	−2.73	−17.18	−10.37	−4.57	−0.68	−6.23
Glide emodel	−22.27	−53.37	−47.10	−31.99	−35.67	−38.07
Glide energy	−22.24	−40.40	−36.53	−27.17	−25.20	−26.53
Glide einternal	0.91	7.42	3.08	6.32	5.32	5.21
Glide posenum	134	29	166	338	359	74
SARS-CoV-2	**Diethylstilbestrol**	**Enterodiol**	**Enterolactone**	**Flavokawain A**	**Flavokawain B**	**Flavokawain C**
Docking Score	−4.81	−6.14	−6.76	−5.15	−5.44	−6.07
Glide ligand efficiency	−0.24	−0.28	−0.31	−0.22	−0.26	−0.28
Glide hbond	−0.16	−0.46	−0.46	0.00	0.00	−0.38
Glide evdw	−23.01	−29.46	−29.98	−29.71	−28.49	−23.16
Glide ecoul	−5.75	−11.52	−11.20	−3.01	−3.92	−9.85
Glide emodel	−32.23	−55.43	−55.60	−42.14	−41.28	−46.74
Glide energy	−28.77	−40.98	−41.17	−32.72	−32.41	−33.01
Glide einternal	2.39	4.36	6.66	4.09	2.68	8.01
Glide posenum	344	74	163	259	53	333
HP-5	**Diethylstilbestrol**	**Enterodiol**	**Enterolactone**	**Flavokawain A**	**Flavokawain B**	**Flavokawain C**
Docking Score	−2.85	−4.12	−5.48	−3.34	−3.59	–
Glide ligand efficiency	−0.14	−0.19	−0.25	−0.15	−0.17	–
Glide hbond	−0.20	−0.61	−0.81	−0.07	0.00	–
Glide evdw	−19.22	−22.02	−18.94	−20.69	−23.00	–
Glide ecoul	−2.75	−8.99	−12.04	−1.67	−1.02	–
Glide emodel	−23.62	−37.66	−38.06	−28.80	−30.81	–
Glide energy	−21.97	−31.01	−30.98	−22.36	−24.03	–
Glide einternal	1.74	2.95	6.72	8.23	8.58	–
Glide posenum	177	252	3	20	314	–

3. Results and discussion

3.1. Enzymes

The collagenase and elastase inhibition assays of some phenolic compounds were performed according to the previous studies. These compounds showed excellent to good inhibitory activities against studied these enzymes with IC_{50} values in ranging between 9.66 ± 1.52 to 121.20 ± 15.87 μM for collagenase and 11.06 ± 1.87 to 27.31 ± 4.673 μM for elastase. Standard compounds for these enzymes had IC_{50} values of 101.37 ± 14.76 nM against collagenase and 30.55 ± 3.25 μM against elastase (Table 1). The most potent compounds against collagenase and elastase were compounds Enterolactone and Flavokawain C with IC50 values of 9.66 ± 1.52 and 62.05 ± 9.43 μM against collagenase and IC50 values of Enterodiol and Diethylstilbestrol were 11.06 ± 1.87 and 13.28 ± 2.78 μM against elastase, respectively. Both collagenase and elastase are significant enzymes in the breakdown of connective tissue in arthritis. Collagenase enzyme is particularly destructive in cartilage destruction. Recently, elastase can also degrade collagen. Collagenases are found in many tissues, active or latent, including synovial fluid and tissue. The 'dendritic' cells, especially in the synovium, are a rich source of latent collagenase. Indeed, elastase is found in neutrophil granulocytes, and this enzyme helps destroy articular cartilage in rheumatoid arthritis. The rate of joint destruction is usually rapid in severe inflammatory diseases such as untreated gout or active rheumatoid arthritis, and slower in degenerative joint diseases such as osteoarthrosis [37]. The finding that collagenase harvested from a perforation forms a perforation in an intact alkali-burned cornea and that perforations can be prevented by perfusing alkaline-scorched corneas with combinations of disodium edetic acid and cysteine, known as in vitro collagenase inhibitors, indicated that the enzyme was the cause of these ulcers. Since collagenase has been found to be is present in various types of corneal ulcers and perforations in humans, the importance of finding the best collagenase inhibitor for possible clinical use is clear, and the alkaline burnt cornea seems to be the ideal model for the study [38]. N-(Methoxysuccinyl)-Ala-Ala-Pro-Val-chloromethyl ketone was used as a control compound in the study, IC50 of compounds were better than control compound.

3.2. Molecular docking study

Theoretical calculations now have a great importance in chemistry. For this reason, it has brought great convenience to chemistry with theoretical calculations. Many package programs are used to compare the chemical and biological activities of molecules with theoretical calculations. With the theoretical results obtained as a result of these comparisons, it has become possible to synthesize more effective and more active molecules.

The antioxidant properties of the three molecules with the highest activity in this study were investigated. Gaussian package program was used in these calculations. The anti-oxidant properties of the molecules are calculated by removing the hydrogen bound bond to the oxygen present in the molecule. Its value is given in Table 2.

When examining the anti-oxidant properties of the molecules, one or

Table 4
ADME properties of molecules.

	Diethylstilbestrol	Enterodiol	Enterolactone	Flavokawain A	Flavokawain B	Flavokawain C	Reference Range
mol_MW	268	302	298	314	284	300	130–725
dipole (D)	0.0	5.7	4.2	2.8	2.9	3.8	1.0–12.5
SASA	539	571	504	587	553	565	300–1000
FOSA	187	106	109	286	194	194	0–750
FISA	109	191	148	70	70	124	7–330
PISA	242	275	247	232	289	247	0–450
WPSA	0	0	0	0	0	0	0–175
volume (A^3)	942	1003	925	1016	945	967	500–2000
donorHB	2	4	2	0	0	1	0–6
accptHB	1.5	4.9	4.5	4.0	3.3	4.0	2.0–20.0
glob (Sphere = 1)	0.9	0.8	0.9	0.8	0.8	0.8	0.75–0.95
QPpolrz (A^3)	29.4	29.5	29.4	31.6	29.9	29.8	13.0–70.0
QPlogPC16	9.9	11.7	10.3	9.7	9.5	10.0	4.0–18.0
QPlogPoct	13.1	18.6	15.3	12.0	11.2	13.3	8.0–35.0
QPlogPw	6.3	12.5	9.7	5.4	5.1	7.2	4.0–45.0
QPlogPo/w	5.1	2.0	2.4	3.8	3.7	3.1	−2.0–6.5
QPlogS	−4.1	−2.8	−2.9	−4.3	−3.8	−3.8	−6.5–0.5
CIQPlogS	−4.6	−3.9	−4.3	−4.6	−4.3	−4.4	−6.5–0.5
QPlogHERG	−4.9	−5.3	−4.1	−5.3	−5.5	−5.3	[a]
QPPCaco (nm/sec)	915	154	390	2155	2155	655	[b]
QPlogBB	−0.8	−1.9	−1.0	−0.6	−0.5	−1.1	−3.0–1.2
QPPMDCK (nm/sec)	450	66	179	1134	1134	313	[b]
QPlogKp	−2.0	−3.0	−2.8	−1.2	−1.1	−2.2	Kp in cm/hr
IP (ev)	9.1	9.1	9.3	9.0	9.3	9.1	7.9–10.5
EA (eV)	−0.2	0.0	0.0	0.7	0.8	0.8	−0.9–1.7
#metab	4	6	5	4	3	4	1–8
QPlogKhsa	0.5	−0.2	0.0	0.2	0.2	0.1	−1.5–1.5
Human Oral Absorption	3	3	3	3	3	3	–
Percent Hum. Oral Absorp.	97	78	87	100	100	95	[c]
PSA	45	88	84	67	59	81	7–200
RuleOfFive	1	0	0	0	0	0	Maximum is 4
RuleOfThree	0	0	0	0	0	0	Maximum is 3
Jm	0.2	0.5	0.6	2.1	3.1	0.3	-

[a] (corcern below −5).
[b] <25 is poor and >500 is great.
[c] <25% is poor and >80% is high.

Table 5
In vitro anti-proliferative activities of Diethylstilbestrol, Enterodiol, Enterolactone, Flavokawain A, Flavokawain B, and Flavokawain C compounds against human cancer cell lines.

NO	Compounds	SK-LU-1	SPC-A-1	95D
		IC50 (μM)	IC_{50} (μM)	IC_{50} (μM)
1	Diethylstilbestrol	15.02	12.76	17.36
2	Enterodiol	67.31	61.05	64.07
3	Enterolactone	45.84	42.17	41.12
4	Flavokawain A	23.27	19.06	22.45
5	Flavokawain B	29.31	31.73	32.62
6	Flavokawain C	22.66	25.01	20.98
	Doxorubicin*	25	30	25

more hydroxyl groups can be found in the skeletal structure of the molecule. The molecular structures of the molecules are given in Figure Figs. 2, 3, and 4. All atoms are labeled. The numerical value of the bond dissociation enthalpy (BDE) energy of the OH bond of molecules is related to the HAT mechanism. It has been observed that the molecule with a lower numerical value of the bond dissociation enthalpy (BDE) energy of the molecule has a higher radical-scavenging activity.

In the first mechanism of SET-PT of molecules, the ionization potential energy value can be calculated. It is easier for a molecule with a low numerical value of this parameter to donate electrons. In the SET-PT second mechanism of molecules, the proton dissociation enthalpy energy value of the molecules is calculated. If the proton dissociation enthalpy energy value of the molecules is lower, the reaction proceeds more easily. Another mechanism, SPLET mechanism, consists of two stages. In the first stage, the proton affinity energy value is calculated. If the proton affinity energy value of a molecule is lower, it shows that the molecule has a high proton affinity. In the two stages of the SPLET mechanism, the electron transfer enthalpy energy value of the molecules is calculated. If the numerical value of the electron transfer enthalpy (ETE) energy of the molecule is lower, the reaction will be easier to proceed. All parameters calculated as a result of the calculations are given in Table 1.

As a result of the anti-oxidant calculations, spin density calculations were made to calculate the charge densities of the molecules with the hydrogen atom removed. The values obtained as a result of these calculations are given on the atoms in Figs. 5–7.

After theoretical calculations, the activities of molecules against enzyme proteins were compared. In this comparison, it has been seen that the interaction of molecules with enzyme proteins causes them to increase their activity. The docking score parameter of molecules is used to compare the activities of molecules in docking calculations. The molecule with the most negative numerical value of the docking score parameter has higher biological activity. The increase in interaction between molecules and proteins makes the numerical value of this parameter more negative [39,40].

After theoretical calculations, the activities of compounds against enzyme proteins were compared. In this comparison, it has been seen that the interaction of compounds with enzyme proteins causes them to increase their activity. The docking score parameter of compounds is used to compare the activities of molecules in docking calculations. The compound with the most negative numerical value of the docking score parameter has higher biochemical activity. The increase in interaction between molecules and proteins makes the numerical value of this parameter more negative. Indeed, these interactions have good interactions like polar, π-π, hydrophobic interactions, hydrogen bonds, and halogen [41,42]. The interactions of molecules with the highest

activity with proteins are given in Figs. 8–11. The numerical values of all parameters of this interaction are given in Table Tables 3 and 4.

After these interactions patterns, ADME/T calculations were made to examine how these molecules act in human metabolism. With these calculations, he examines the uptake of molecules into human metabolism, their movements for metabolism, their effects and reactions, and finally their excretion from human metabolism [43,44].

Many other parameters are used to explain the exposure and interactions that occur between molecules and proteins. As a result of the ADME/T calculations, it was seen that the numerical values of the parameters found for the studied molecules were within the desired range. As a result, the molecules studied are suitable for future use as drugs [45].

3.3. Anti-cancer results

The compounds of Diethylstilbestrol, Enterodiol, Enterolactone, Flavokawain A, Flavokawain B, and Flavokawain C were screened in vitro for their antcancer anticancer activities against SPC-A-1, SK-LU-1, and 95D human lung cancer cell lines, with the anticancer drug Doxorubicin used as a control compound. Indeed, in vitro anticancer screening methods were conducted at various compound concentrations. All of the experiments were carried out in triplicate. Additionally, the IC_{50} values were calculated from the percentage of anticancer effect by nonlinear curve fitting and are presented in Table 5. In this part, between all of the investigated molecules, Diethylstilbestrol, Flavokawain A, Flavokawain C and Flavokawain B exhibited the most potent growth inhibition in the three lung cancer cells, with an IC_{50} value of 12–30 μM, indicating that they are more potent than Doxorubicin, which exhibited an IC_{50} value of 25–30 μM. Also, other molecules exhibited significantly weaker activity, because the anticancer was lower than that of Doxorubicin in the three cell lines, with an IC_{50} value of 30–70 μm (Table 5).

4. Conclusions

In this study, among the molecules that we successfully investigated, compounds Diethylstilbestrol, Flavokawain C, Flavokawain A and Flavokawain B had a strong electron-withdrawing group in the phenyl ring with the highest cytotoxic activity against the cancer cell lines tested. On the other hand, the four molecules had lung-anticancer potentials, and they may used use as anti-collagenase and anti-elastase drugs design. The results of the theoretical calculations made showed that both DFT calculations and molecular docking calculations were found to be in great agreement with the experimental results. This study is an important reference for future *in vivo* and in vitro studies.

Data availability statement

The data that support the findings of this study are available from the corresponding author upon reasonable request.

Declaration of competing interest

There isn't any conflict of Interest.

References

[1] O. Wakabayashi, K. Yamazaki, S. Oizumi, F. Hommura, I. Kinoshita, S. Ogura, CD4þ T cells in cancer stroma, not CD8þ T cells in cancer cell nests, are associated with favorable prognosis in human non-small cell lung cancers, Cancer Sci. 94 (2003) 1003–1009.

[2] L.E. Raez, S. Fein, E.R. Podack, Lung cancer immunotherapy, Clin. Med. Res. 3 (2005) 221–228.

[3] M. Guo, G.B. Ding, P. Yang, L. Zhang, H. Wu, H. Li, Z. Li, Migration suppression of small cell lung cancer by polysaccharides from nostoc commune vaucher, J. Agric. Food Chem. 64 (2016) 6277–6285.

[4] G.D. Yao, J. Yang, Q. Li, Y. Zhang, M. Qi, S.M. Fan, T. Hayashi, S. Tashiro, S. Onodera, T. Ikejima, Activation of p53 contributes to pseudolaric acid B-induced senescence in human lung cancer cells in vitro, Acta Pharmacol. Sin. 37 (2016) 919–929.

[5] B. Castro-Carvalho, A.A. Ramos, M. Prata-Sena, F. Malhao, M. Moreira, D. Gargiulo, T. Dethoup, S. Buttachon, A. Kijjoa, E. Rocha, Marine-derived fungi extracts enhance the cytotoxic activity of Doxorubicin in nonsmall cell lung cancer cells A459, Pharmacogn. Res. 9 (2017) S92–S98.

[6] R. Bingula, C. Dupuis, C. Pichon, J.Y. Berthon, M. Filaire, L. Pigeon, E. Filaire, Study of the effects of betaine and/or C-phycocyanin on the growth of lung cancer A549 cells in vitro and in vivo, JAMA Oncol. 2016 (2016), 8162952.

[7] B. Li, M.H. Gao, X.M. Chu, L. Teng, C.Y. Lv, P. Yang, Q.F. Yin, The synergistic antitumor effects of all-trans retinoic acid and C-phycocyanin on the lung cancer A549 cells in vitro and in vivo, Eur. J. Pharmacol. 749 (2015) 107–114.

[8] K.K. Lee, J.H. Kim, J.J. Cho, J.D. Choi, Inhibitory Effects of 150 plant extracts on elastase activity, and their anti-inflammatory effects, Int. J. Cosmet. Sci. 21 (1999) 71–82.

[9] B. Siedle, S. Cisielski, R. Murillo, B. Löser, V. Castro, C.A. Klaas, O. Hucke, A. Labahn, M.F. Melzig, I. Merfort, Sesquiterpene lactones as inhibitors of human neutrophil elastase, Bioorg. Med. Chem. 10 (2002) 2855–2861.

[10] M.F. Melzig, B. Löser, S. Ciesielski, Inhibition of neutrophil elastase activity by phenolic compounds from plants, Pharmazie 56 (2001) 967–970.

[11] S. Baylac, P. Racine, Inhibition of human leukocyte elastase by natural fragrant extracts of aromatic plants, Int. J. Aromather. 14 (2004) 179–182.

[12] R. Bauer, K. Janowska, K. Taylor, B. Jordan, S. Gann, T. Janowski, J. Sakon, Acta Crystallogr. Sect. D Biol. Crystallogr. 71 (3) (2015) 565–577.

[13] J. Vijayalakshmi, E.F. Meyer Jr., C.M. Kam, J.C. Powers, Structural study of porcine pancreatic elastase complexed with 7-amino-3- (2-bromoethoxy) -4-chloroisocoumarin as a nonreactivatable doubly covalent enzyme-inhibitor complex, Biochemistry 30 (8) (1991) 2175–2183.

[14] Z. Jin, Y. Zhao, Y. Sun, B. Zhang, H. Wang, Y. Wu, Z. Rao, Structural basis for the inhibition of SARS-CoV-2 main protease by antineoplastic drug carmofur, Nat. Struct. Mol. Biol. 27 (6) (2020) 529–532.

[15] J.P. Declercq, C. Evrard, A. Clippe, D. Vander Stricht, A. Bernard, B. Knoops, Crystal structure of human peroxiredoxin 5, a novel type of mammalian peroxiredoxin at 1.5 Å resolution, J. Mol. Biol. 311 (4) (2001) 751–759.

[16] D.E. Gordon, et al., A SARS-CoV-2-human protein-protein interaction map reveals drug targets and potential drug-repurposing, bioRxiv (2020) 2020, 03.22.002386.

[17] Anti-collagenase, anti-elastase and anti-oxidant activities of extracts from 21 plants tamsyn SA thring, pauline Hili, and Declan P naughton, BMC Compl. Alternative Med. 9 (2009) 27, https://doi.org/10.1186/1472-6882-9-27.

[18] E. Barrantes, M. Guinea, Inhibition of collagenase and metalloproteinases by aloins and aloe gel, Life Sci. 72 (2003) 843–850.

[19] H.E. Van Wart, D.R. Steinbrink, A continuous spectrophotometric assay for Clostridium histolyticum collagenase, Anal. Biochem. 113 (1981) 356–365.

[20] J.Y. Moon, E.Y. Yim, G. Song, N.H. Lee, C.G. Hyun, Screening of elastase and tyrosinase inhibitory activity from Jeju Island plants, EurAsia J. BioSci. 4 (2010) 41–53.

[21] G.D. Liyanaarachchi, J.K.R.R. Samarasekera, K.R.R. Mahanama, K.D.P. Hemalal, Tyrosinase, elastase, hyaluronidase, inhibitory and antioxidant activity of Sri Lankan medicinal plants for novel cosmeceuticals, Ind. Crop. Prod. 111 (2018) 597–605.

[22] A. Sahasrabudhe, M. Deodhar, Anti-hyaluronidase, anti-elastase activity of *Garcinia indica*, Int. J. Bot. 6 (2010) 299–303.

[23] J. Wittenauer, S. Mäckle, D. Sußmann, U. Schweiggert-Weisz, R. Carle, Inhibitory effects of polyphenols from grape pomace extract on collagenase and elastase activity, Fitoterapia 101 (2015) 179–187.

[24] Z. Marković, S. Jeremić, J.D. Marković, M.S. Pirković, D. Amić, Influence of structural characteristics of substituents on the antioxidant activity of some anthraquinone derivatives, Computational Theoretical Chem. 1077 (2016) 25–31.

[25] S. Sari, B. Barut, A. Özel, D. Şöhretoğlu, Tyrosinase inhibitory effects of Vinca major and its secondary metabolites: enzyme kinetics and in silico inhibition model of the metabolites validated by pharmacophore modelling, Bioorg. Chem. 92 (2019), 103259.

[26] E. Koç, A. Üngördü, F. Candan, Antioxidant properties of methanolic extract of 'Veronica multifida'and DFT and HF analyses of its the major flavonoid component, J. Mol. Struct. 1197 (2019) 436–442.

[27] A. Urbaniak, M. Szeląg, M. Molski, Theoretical investigation of stereochemistry and solvent influence on antioxidant activity of ferulic acid, Computational Theoretical Chem. 1012 (2013) 33–40.

[28] R. Kheirabadi, M. Izadyar, Antioxidant activity of selenenamide-based mimic as a function of the aromatic thiols nucleophilicity, a DFT-SAPE model, Comput. Biol. Chem. 75 (2018) 213–221.

[29] J.S. Wright, E.R. Johnson, G.A. DiLabio, Predicting the activity of phenolic antioxidants: theoretical method, analysis of substituent effects, and application to major families of antioxidants, J. Am. Chem. Soc. 123–6 (2001) 1173–1183.

[30] J.E. Bartmess, Thermodynamics of the electron and the proton, J. Phys. Chem. 98–25 (1994) 6420–6424.

[31] L. Schrodinger, Small-Molecule Drug Discovery Suite 2019-4, 2019.

[32] M.J. Frisch, G.W. Trucks, H.B. Schlegel, G.E. Scuseria, M.A. Robb, J.R. Cheeseman, G. Scalmani, V. Barone, B. Mennucci, G.A. Petersson, H. Nakatsuji, M. Caricato, X. Li, H.P. Hratchian, A.F. Izmaylov, J. Bloino, G. Zheng, J.L. Sonnenberg, M. Hada, M. Ehara, K. Toyota, R. Fukuda, J. Hasegawa, M. Ishida, T. Nakajima, Y. Honda, O. Kitao, H. Nakai, T. Vreven, J.A. Montgomery, J.E. Peralta, F. Ogliaro, M. Bearpark, J.J. Heyd, E. Brothers, K.N. Kudin, V.N. Staroverov, R. Kobayashi, J. Normand, K. Raghavachari, A. Rendell, J.C. Burant, S.S. Iyengar, J. Tomasi,

M. Cossi, N. Rega, J.M. Millam, M. Klene, J.E. Knox, J.B. Cross, V. Bakken, C. Adamo, J. Jaramillo, R. Gomperts, R.E. Stratmann, O. Yazyev, A.J. Austin, R. Cammi, C. Pomelli, J.W. Ochterski, R.L. Martin, K. Morokuma, V.G. Zakrzewski, G.A. Voth, P. Salvador, J.J. Dannenberg, S. Dapprich, A.D. Daniels, O. Farkas, J. B. Foresman, J.V. Ortiz, J. Cioslowski, D.J. Fox, Gaussian 09, Revision D.01, Gaussian Inc, Wallingford CT, 2009.

[33] Schrödinger Release 2019-4, LigPrep, Schrödinger, LLC, New York, NY, 2019.

[34] Schrödinger Release 2019-4: Protein Preparation Wizard; Epik, Schrödinger, LLC, New York, NY, 2016; Impact, Schrödinger, LLC, New York, NY, 2016; Prime, Schrödinger, LLC, New York, NY, 2019.

[35] Schrödinger Release 2020-1, QikProp, Schrödinger, LLC, New York, NY, 2020.

[36] L. Kupcsik, Estimation of cell number based on metabolic activity: the MTT reduction assay, Methods Mol. Biol. 740 (2011) 13–19.

[37] S. Sadeghi-Kaji, B. Shareghi, A.A. Saboury, S. Farhadian, Spectroscopic and molecular docking studies on the interaction between spermidine and pancreatic elastase, Int. J. Biol. Macromol. 131 (2019) 473–483.

[38] G.D. Liyanaarachchi, J.K.R.R. Samarasekera, K.R.R. Mahanama, K.D.P. Hemalal, Tyrosinase, elastase, hyaluronidase, inhibitory and antioxidant activity of Sri Lankan medicinal plants for novel cosmeceuticals, Ind. Crop. Prod. 111 (2018) 597–605.

[39] S.B. Al Rihani, et al., Risk of adverse drug events following the virtual addition of COVID-19 repurposed drugs to drug regimens of frail older adults with polypharmacy, J. Clin. Med. 9 (2020) 2591.

[40] S. Dotolo, A. Marabotti, A. Facchiano, R. Tagliaferri, A review on drug repurposing applicable to COVID-19. Brief, Bioinformatics 22 (2021) 726–741.

[41] Y. Zhou, et al., Network-based drug repurposing for novel coronavirus 2019-nCoV/SARS-CoV-2, Cell Discov 6 (2020) 1–18.

[42] D.E. Gordon, et al., A SARS-CoV-2 protein interaction map reveals targets for drug repurposing, Nature 583 (2020) 459–468.

[43] F. Tok, B. Koçyiğit-Kaymakçıoğlu, B.N. Sağlık, S. Levent, Y. Özkay, Z. A. Kaplancıklı, Synthesis and biological evaluation of new pyrazolone Schiff bases as monoamine oxidase and cholinesterase inhibitors, Bioorg. Chem. 84 (2019) 41–50.

[44] U.A. Çevik, D. Osmaniye, S. Levent, B.N. Sağlik, B.K. Çavuşoğlu, Y. Özkay, Z. A. Kaplancikl, Synthesis and characterization of a new series of thiadiazole derivatives as potential anticancer agents, Heterocycl. Commun. 26 (1) (2020) 6–13.

[45] Y. Wang, et al., In silico ADME/T modelling for rational drug design, Q. Rev. Biophys. 48 (2015) 488–515, https://doi.org/10.1017/S0033583515000190.